SYNCHROTRON X-RAYS FOR STRUCTURAL CHARACTERIZATION OF STAINLESS STEELS

P. Hedström[1], M. Odén[2]

[1]Luleå University of Technology, Sweden, [2]Linköping University, Sweden

Abstract

High-energy x-rays as produced from one of the three large scale synchrotron sources world wide have the capacity to penetrate millimeters of stainless steel and thus it provides a suitable probe for bulk characterization. Further, the high brilliance of the x-rays enable kinetic studies and the possibility to probe the meso-scale structure such as single grains and dislocation structures embedded in the steels. The current paper provides an overview of the work conducted using synchrotron x-rays for structural characterization of stainless steels. Synchrotron x-ray characterization is also discussed in the light of other experimental techniques. We provide scientific examples of synchrotron x-ray diffraction studies on metastable austenitic and duplex stainless steel taken from our own work, and additional examples from the literature are given. When looking at the recently published literature many new insights in metal behavior have been gained by the utilization of synchrotron x-ray characterization. However, this type of research has only started and we predict more frequent usage and that these techniques will contribute significantly to the advance of our current understanding of polycrystalline metals, e.g. stainless steels.

Introduction

The relationship between microstructure and material properties is fundamental in material science, and the progress in material science is often related to improvements or discoveries of new experimental techniques. For instance, the advent of x-ray diffraction in the early 1900s has markedly changed our conception of materials crystallography. Moreover, the transmission-electron microscopes frequently becoming used in the mid 1900s have given us a much better understanding of e.g. defect structures. Most common experimental techniques for structural characterization are however surface techniques, where conventional x-ray diffractometry and scanning electron microscopy are both restricted to the near surface, and in stainless steel the penetration depth is limited to a few μm. Transmission-electron microscopy has even higher limitations concerning the penetration depth and is solely restricted to the investigation of thin foils (~100 nm) [1]. Even though the surface structure of materials is clearly relevant and it can be a good approximation to the interior structure, there are exceptions. For instance, in the case of deformation-induced martensitic phase transformation in stainless steels it is difficult to quantify the phase fractions using a pure surface method [2]. Another example comes from material modeling and concerns the building of the next generation polycrystalline plasticity models. The over simplified traditional models do not take the local neighborhood of single grains into consideration, but this is appreciated in the more recent models which are finite element based [3]. Neighboring grains needs to have compatibility across the grain boundaries and this imposes deformation constraints between the grains. The result is a different deformation behavior between single crystals, bicrystals and polycrystals [4]. The deformation

constraint has mainly been investigated using transmission-electron microscopy and these investigations have contributed to the understanding of compatibility constraint. However, to fully comprehend this behavior in polycrystalline materials it is necessary to investigate the behavior of single grains embedded in an aggregate of grains, i.e. polycrystalline aggregate. Therefore, researchers have for some time searched for experimental techniques capable of probing the meso-scale structure (e.g. single grains and dislocation structures) within the bulk of polycrystals, since this would help in the understanding of polycrystalline materials (e.g. stainless steels). Attention has therefore been given to three-dimensional characterization, where novel techniques have emerged. One of these techniques is the combination of scanning electron microscopy (SEM) and focused ion beam (FIB), where serial sectioning using the FIB enables the collection of images through the depth of a sample by SEM. These images can then be put together to form a three-dimensional micrograph [5]. The high resolution of a Field-emission-gun (FEG)-SEM means that high resolution (~1 nm) three-dimensional micrographs can be recorded. The major drawback is however the destructive nature of the FIB-SEM and it is therefore not possible to conduct kinetic studies. Additional drawbacks for 3D characterization by FIB-SEM are the introduction of radiation damage and limited erosion rate. Another technique which has been around for some time is neutron diffraction. The neutrons have the penetration depth of centimeters in stainless steels and it is thus suitable for three-dimensional characterization, as demonstrated in [6-9]. Moreover, neutron diffraction is non-destructive enabling investigations of microstructure evolution. However, the data acquisition time is rather slow and the spatial resolution of neutron diffraction is not sufficient to probe the meso-scale structure. High-energy x-ray diffraction is an excellent complementary technique to neutron diffraction [10]. These x-rays are capable of penetrating millimeters of stainless steels and for modern steels with μm grain sizes this is a suitable bulk probe. Further, high-energy x-ray diffraction provides considerably better time resolution compared to neutron diffraction and in addition it enables meso-scale structural characterization within the bulk of stainless steels.

The subsequent part of this paper provides an overview of synchrotron x-ray characterization and the work conducted to date on stainless steels. Scientific examples are divided in three categories: phase transformations, residual stresses and single bulk grain behavior. The examples are mainly collected from our own work, but it also comprises an overview of research conducted by other researchers in the field.

Synchrotron x-ray characterization of stainless steels

As mentioned above, high-energy x-ray diffraction has the capacity to fill the gap between some of the more established experimental techniques for structural characterization. The high-energy x-ray diffraction technique cannot compete with the Scanning Probe Microscopy (SPM) concerning spatial resolution, since the SPM has a true atomic spatial resolution in best case. However, SPM is a pure surface probe, while diffracted high-energy x-rays will penetrate millimeters of steel. On the other hand neutrons have better penetration power than high-energy x-rays, but the temporal and spatial resolution is worse.

The characteristics of the high-energy x-rays with a penetration power of about 5 mm at an x-ray energy of 50 keV and a μm spatial resolution has opened up a new field of research. It is the first technique truly capable of probing the meso-scale structure embedded in the bulk of materials. This was first realized by researchers at Risø National Laboratory who developed a technique called three-dimensional x-ray diffraction (3DXRD) in collaboration with researchers at the European Synchrotron Radiation Facility (ESRF). The 3DXRD technique enables characterization of single grains and dislocation structures embedded in the bulk of polycrystals [11-12]. In addition to the high-energy synchrotron facility ESRF in Grenoble, France, there are two more high-energy synchrotron facilities: the Advanced Photon Source (APS) in Argonne, Il,

USA and the Super Photon Ring 8 (SPRing8) in West Harima, Japan. These sources can produce highly energetic x-rays, preferred for bulk studies. The synchrotron x-ray characterization is becoming more accessible to the research community, since many new facilities are being established today. The experiments conducted by Hedström et al. and presented here are all conducted at the 1-ID beamline at the Advanced Photon Source [13]. This undulator beamline is dedicated to high-energy x-ray scattering techniques and it is a versatile beamline where different environments for the sample can be used [14-16]. The measurements presented here are all *in situ* x-ray diffraction measurements during tensile loading of stainless steels and the typical setup is demonstrated in Figure 1. The white x-rays generated from the synchrotron source are made monochromatic and then allowed to pass through the stainless steel sample. The x-rays are scattered in the sample and the diffracted x-rays are collected with an area detector located behind the specimen. Two different types of measurements have been conducted, where the first is average grain measurements as exemplified in the diffraction pattern on the left hand side. The other type of measurement is the single grain measurement, where the x-ray probe is made small to only allow diffraction signal from a few grains as seen in the spotty diffraction pattern on the right hand side.

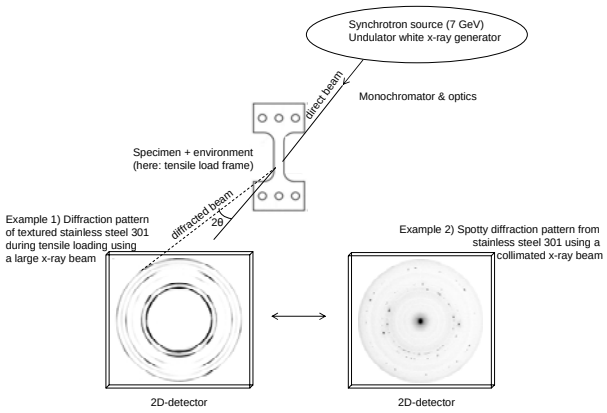

Figure 1. Typical setup for transmission x-ray diffraction

We will in the coming paragraphs present a review of the work conducted to date on stainless steels using synchrotron x-ray diffraction in three areas, namely phase transformations, residual stresses and single bulk grain behavior.

Kinetics of phase transformations

There are quite a few examples of *in situ* characterization of phase transformations in stainless steels. Several of these investigations deal with phase transformations during welding. Elmer et al. used time resolved x-ray diffraction to investigate the solidification in the weld pool of a 304 stainless steel. Their good time resolution of 50 ms provided the first direct proof that δ-ferrite is the first phase to solidify [17]. Elmer and coworkers have further investigated the ferrite, austenite and sigma formation during heating and cooling of duplex stainless steels using synchrotron radiation [18-19]. Feaugas et al. investigated the nitriding of stainless steels surfaces using small-angle x-ray scattering at a synchrotron source. The high brilliance of the x-ray source allowed *in situ* observations of the nitridation process [20]. The formation of a thin passive layer of chromium-oxide on the surface of stainless steels was investigated by photoelectron spectroscopy with a tailored synchrotron x-ray beam to see chromium and iron [21]. The strain-induced martensitic phase transformation in metastable austenitic stainless steels has been investigated in [22]. The effect of cold rolling reduction and different strain rates on the strain-induced martensitic transformation and the mechanical properties of a 301 stainless steel were investigated. Autocatalytic martensitic transformation triggered by strains from the transformation itself could be observed at high applied strains, and this autocatalytic

transformation contributes significantly to the ductility of the steel [13]. Further, the load sharing between austenite and α'-martensite could be determined *in situ* during loading and this provided sound data for evaluation of material modeling of the load response of 301 stainless steel [23].

Residual stress evolution

The residual stresses in the bulk of stainless steels have been examined by a number of authors using neutron diffraction [e.g. 24-25]. Synchrotron x-ray residual stress characterization is more scarce in the literature, but Hedström et al. have investigated the residual stress evolution during tensile loading for cold rolled stainless steel 301 using synchrotron x-ray diffraction [26]. In addition, the lattice strain evolution during *in situ* continuous tensile loading was followed. The results showed that the harder α'-martensite phase is put in a tensile residual stress state along the rolling direction after cold rolling. Balancing compressive residual stress in the austenite phase was found. The opposite residual stress state was found in α'-martensite and austenite transverse to the rolling direction. The hkl-dependent lattice strain evolution was also determined and the significant differences between crystallographic planes were noticed, which is an important aspect to consider in the residual stress determination from x-ray diffraction data.

Single bulk grain behavior

The three-dimensional x-ray diffraction technique has been used for some recent scientific highlights [27-29]. For instance, the transformation of single bulk grains from austenite to ferrite was followed during cooling of a carbon steel [28] and recrystallization of single bulk grains during heating of an aluminum specimen was investigated [29]. However, the only investigations on single bulk grains in stainless steels are gathered in [22]. Hedström et al. investigated the elastic strain tensor evolution of 15 single bulk grains during tensile loading of a duplex stainless steel [30]. Hedström et al. also investigated the elastic strain tensor evolution of single bulk grains in 301 stainless steel during tensile loading. The elastic strain evolution of 7 austenite grains up to 5% applied strain and the formation of ε-martensite in one of them was reported [31]. Further, another sample was loaded to 20% applied strain and it was possible to follow the rotation of 7 austenite grains and the formation of α'-martensite in two of the austenite grains [32].

Outlook

The continuous development to improve state-of-the-art synchrotron facilities and equipment will continue to push the boundaries for materials characterization. As reviewed in this paper it is possible to conduct true three-dimensional characterization with a time resolution on the order of milliseconds and a spatial resolution on the order of μm. The near future holds further advance and a nano-scope is currently being developed at the ESRF in Grenoble [33]. Thus it is likely to enable advanced experiments where the fundamentals of nano-materials (e.g. precipitation hardened stainless steels with nano-precipitates) can be tested. The even higher brilliance of the x-ray sources and foremost the better detectors will improve time resolution and provide even better time resolved kinetic studies. Currently the free-electron laser x-ray sources are being commissioned and already totally novel experiments with time resolutions down to femtoseconds has been conducted. Moreover, at this point in time steps are taken to build a new synchrotron source in Sweden (MAX IV) that would cater primarily to Scandinavian users with one dedicated beamline for the type of work outlined in this paper [34]. To summarize, the x-ray diffraction results presented here from work conducted at synchrotron facilities is just the beginning of the development where traditional materials such as stainless steels will be reinvestigated in the light of better experimental methods and this will improve our current understanding of these materials.

Acknowledgement

Ulrich Lienert and Jon Almer are gratefully acknowledged for general support during experiments and analysis. Mark Terner and Joel Bernier are thanked for assistance during synchrotron experiments and the financial support from the Swedish Research Council and Outokumpu Research Foundation is gratefully acknowledged. The use of the Advanced Photon Source was supported by the U. S. Department of Energy, Office of Science, Office of Basic Energy Sciences, under Contract No. W-31-109-Eng-38 and DE-AC02-06CH11357.

References

[1] P.J. Goodhew, J. Humphreys, R. Beanland: “Electron microscopy and analysis”, 3rd edition, Taylor and Francis, 2001, London, UK

[2] J. Talonen, P. Aspegren, H. Hänninen: “Comparison of different methods for measuring strain induced alpha '-martensite content in austenitic steels”, Mat Sci. Tech., 20, 12, 2004, pp. 1506-1512

[3] U. Lienert, T-S. Han, J. Almer, P.R. Dawson, T. Leffers, L. Margulies, S.F. Nielsen, H.F. Poulsen, S. Schmidt: “Investigating the effect of grain interaction during plastic deformation of copper”, Acta Mater., 52, 2004, pp. 4461-4467

[4] T.H. Courtney: “Mechanical behaviour of materials, 2nd edition, McGraw-Hill, 2000, Singapore

[5] N. Chawla, V.V. Ganesh, B. Wunsch: “Three-dimensional (3D) microstructure visualization and finite element modelling of the mechanical behavior of SiC particle reinforced aluminium composites, Scripta Mater., 51, 2004, pp. 161-165

[6] B. Clausen, T. Lorentzen, M.A.M Bourke, M.R. Daymond: “Lattice strain evolution during uniaxial tensile loading of stainless steel”, Mat. Sci. Eng. A, 259, 1999, pp. 17-24

[7] M.R. Daymond, C.N. Tomé, M.A.M. Bourke: “Measured and predicted intergranular strains in textured austenitic steel”, Acta Mater., 48, 2000, pp. 553-564

[8] M.R. Daymond, P.J. Bouchard: “Elastoplastic deformation of 316 stainless steel under tensile loading at elevated temperatures” Met. Mat. Trans. A, 37A, 2006, pp. 1863-1873

[9] J.W.L. Pang, T.M. Holden, J.S. Wright, T.E. Mason: ”The generation of intergranular strains in 309H stainless steel under uniaxial loading”, Acta Mater., 48, 2000, pp. 1131-1140

[10] J. Almer, U. Lienert, R.L. Peng, C. Schlauer and M. Oden: “Strain and texture analysis of coatings using high-energy x-rays”, J. Appl. Phys. 94, 1, 2003, pp. 697-702

[11] H.F. Poulsen, S. Garbe, T. Lorentzen, D.J. Jensen, F.W. Poulsen, N.H. Andersen, T. Frello, R. Feidenhans´l, H. Graafsma: “Applications of high-energy synchrotron radiation for structural studies of polycrystalline materials”, J. Synch. Rad., 4, 1997, pp. 147-154

[12] E.M. Lauridsen, S. Schmidt, R.M. Suter, H.F. Poulsen: “Tracking: a method for structural characterization of grains in powders or polycrystals”, J. Appl. Cryst., 34, 2001, pp. 744-750

[13] D.R. Haeffner, J.D. Almer, U. Lienert: “The use of high energy x-rays from the Advanced Photon Source to study stresses in materials”, Mat. Sci. Eng. A, 399, 2005, pp. 120-127

[14] B. Jakobsen, H.F. Poulsen, U. Lienert, W. Pantleon: “Direct determination of elastic strains and dislocation densities in individual subgrains in deformation structures”, Acta Mater., 55, 2007, pp. 3421-3430

[15] M. Terner, P. Hedström, J Almer, J. Illavsky, M Odén: ”Residual stress evolution during decomposition of Ti(1-x)Al(x)N coatings using high-energy x-rays” Mat. Sci. For., 524-525, 2006, pp. 619-624

[16] P. Hedström, U. Lienert, J. Almer, M. Odén: “Stepwise transformation behavior of the strain induced martensitic transformation in a metastable stainless steel”, Scr. Mat., 55, 2007, 213-216

[17] J.W. Elmer, J. Wong, T. Ressler: “In-situ observations of phase transformations during solidification and cooling of austenitic stainless steel welds using time-resolved x-ray diffraction”, Scr. Mat., 43, 2000, pp. 751-757
[18] T.A. Palmer, J.W. Elmer, J. Wong: “*In situ* observations of ferrite-austenite transformations in duplex stainless steel weldments using synchrotron radiation”, Sci. Tech. Weld. Join., 7, 3, 2002, pp. 159-171
[19] J.W. Elmer, T.A. Palmer, E.D. Specht: “In situ observations of sigma phase dissolution in 2205 duplex stainless steel using synchrotron radiation”, Mat. Sci. Eng. A, 459, 2007, pp. 151 – 155
[20] J. Feugeas, B. Gómez, A Craievich: “Ion nitriding of stainless steels. Real time surface characterization by synchrotron x-ray diffraction”, Surf. Coat. Tech., 154, 2002, pp. 167 – 175
[21] T.H. Kang et al.: “Direct image observations of the initial forming of passive thin film on stainless steel surface by PEEM”, Appl. Surf. Sci., 212-213, 2003, pp. 630 – 635
[22] P. Hedström: “Deformation and martensitic phase transformation in stainless steels”, PhD thesis, Luleå University of Technology, Luleå, Sweden, 2007, ISSN:1402-1544, http://epubl.ltu.se/1402-1544/67
[23] P. Hedström, L.-E. Lindgren, J. Almer, U. Lienert, J. Bernier, M. Terner, M. Odén: ”Load partitioning and strain-induced martensite formation during tensile loading of a metastable austenitic stainless steel”, communicated
[24] Y.D. Wang, R.L. Peng, X.L. Wang, R.L. McGreevy: “Grain-orientation-dependent residual stress and the effect of annealing in cold rolled stainless steel”, Acta Mater., 50, 2002, pp. 1717-1734
[25] S. Harjo, Y. Tomota, M. Ono: “Measurements of thermal residual elastic strains in ferrite-austenite Fe-Cr-Ni alloys by neutron and x-ray diffraction”, Acta Mater., 47, 1999, pp. 353-362
[26] P. Hedström, J. Almer, U. Lienert, M. Odén: “Evolution of residual strains in metastable austenitic stainless steels and the accompanying strain induced martensitic transformation”, Mat. Sci. Forum, 524-525, 2006, pp. 821-826
[27] B. Jakobsen, H.F. Poulsen, U. Lienert, J. Almer, S.D. Shastri, H.O. Soerensen, C. Gundlach, W. Pantleon: “Formation and subdivision of deformation structures during plastic deformation”, Science, 312, 2006, pp. 889-892
[28] S.E. Offerman, N.H. Dijk, J. van Sietsma, S. Grigull, E.M. Lauridsen, L. Margulies, H.F. Poulsen, M.Th. Rekveldt, S. van der Zwaag: “Grain nucleation and growth during phase transformations”, Science, 298, 2002
[29] L. Margulies, G. Winther, H.F. Poulsen: “In situ measurements of grain rotation during deformation of polycrystals”, Science, 291, 2001
[30] P. Hedström, T.-S. Han, U. Lienert, J. Almer, M. Odén: ”Load partitioning between 15 individual austenite and ferrite grains embedded in the bulk of a duplex stainless steel during tensile loading”, manuscript
[31] P. Hedström, U. Lienert, J. Almer, M. Odén: “Elastic strain evolution and epsilon-martensite formation in individual austenite grains during in situ tensile loading of a metastable stainless steel”, Mat. Let., 2, 31, 2008, pp. 338-340
[32] P. Hedström, U. Lienert, J. Almer, M. Terner, M. Odén: “α’-martensite formation in individual bulk austenite grains during tensile loading of a metastable austenitic stainless steel”, manuscript
[33] D. Juul Jensen, E.M. Lauridsen, L. Margulies, H.F. Poulsen, S. Schmidt, H.O. Sorensen, G.B.M. Vaughan: ”X-ray microscopy in four dimensions”, Materials Today, 9, 2006, pp. 18-25
[34] http://www.maxlab.lu.se/maxlab/max4/index.html

BEHAVIOR AND FORMING LIMIT DIAGRAM PREDICTIONS OF STAINLESS STEELS SHEETS

G. Chinouilh, F. Toscan, J. Leseux, P.O. Santacreu

ArcelorMittal Stainless Europe, France

Abstract

The development of adapted design tools and the use of finite element analysis (FEA) for the forming simulation have helped to increase the use of stainless steels in automotive or other applications like appliances. The behaviour in forming can be well described by the knowledge of a stress-strain curve and the anisotropy of the material, especially in the case of ferritic grades or stable austenitic grades. In the case of unstable austenitic grades an other effort was undertaken to propose a behavior model for the transformation induced plasticity (TRIP)- effect. In fact, strain-rate and consequently temperature gradient may have a significant influence on the hardening of unstable stainless steels and consequently on their forming and crash behavior. The thermo-metallurgical-mechanical model uses a minimum number of parameters: form transformation kinetic and strain-stress curves, determined in isothermal conditions. The proposed model did not lead to any restriction on the description of the strain-stress law and consequently could be easily implemented in FEA software. For fracture prediction, Forming Limit Diagrams (FLD) are now in widespread use to evaluate the feasibility of a stamped part. However, they still present the major drawback of a test-intensive determination procedure. In particular, experimental FLD needs to be determined for each thickness, different strain path and finally be reproduced to evaluate the scattering. The author presents a Cayssials-type analytical model, which describes FLD as a strain instability during biaxial loading and permits to predict it from strain hardening properties. Ultimately, the knowledge of mechanical properties, anisotropy and the thickness of the sheet are simply required for an accurate FLD prediction.

Behavior model for Unstable Austenitic Steels

Trip-Effect

The figure 1a shows conventional tensile curves of unstable austenitic stainless steels for different testing conditions and exhibit two main features :

- an non-constant strain hardening coefficient, leading to some difficulty in fitting such curve with the classical Hollomon or Ludwig models.
- a strong temperature and strain rate sensitivity .

The mechanical behavior of Austenitic stainless steel is linked to austenite stability. Under certain circumstances, the austenite phase has the capability to transform itself into martensite when it is deformed. This metallurgical transformation leads to a particular mechanical behavior designated as the TRIP effect (TRansformation Induced Plasticity). As is the case for most metallurgical transformations, any temperature variation can influence the transformation rate. Consequently, the TRIP-effect has to be taken into account for the modeling of forming and crash behavior.

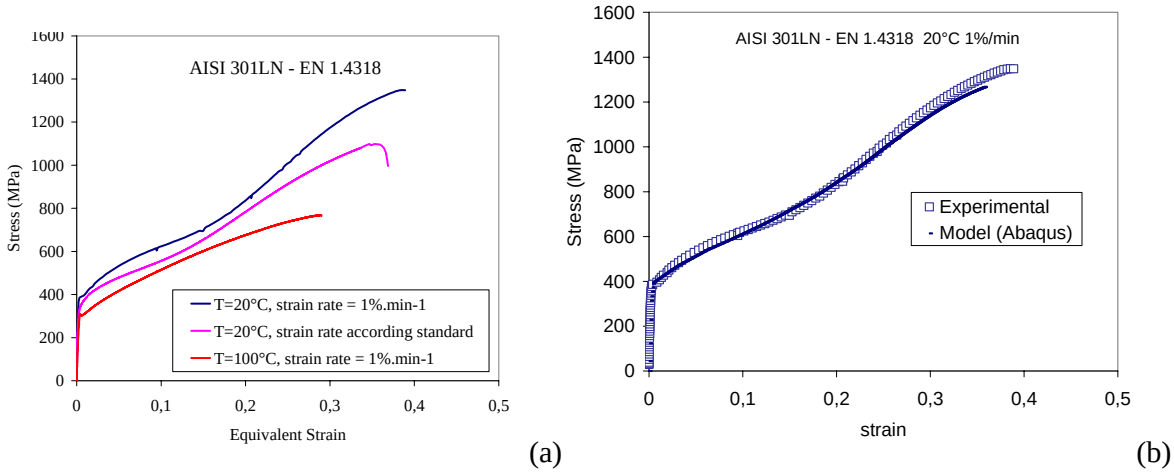

(a) (b)

Figure 1. (a) strain-stress curves on a 1.4318 unstable austenitic grade
(b) comparison between the proposed model and the experiment

The proposed model

In order to simulate the TRIP-effect, a model has been developed by ArcelorMittal Stainless that couples both metallurgical and thermo-mechanical laws:

- kinetics of the martensite transformation induced by the deformation (metallurgical aspect); using Olson&Cohen or Guimaeres equations which relate martensite fraction to the strain and temperature.
- thermal equations describing latent heat generated by the transformation, the plastic work transforming into heat.
- mechanical equations of behavior of a micro-structures containing both austenite and
- α'-martensite by the use of a mix-law.

The development of such a model was performed using an original isothermal tensile test on gridded specimens. So different levels of strain are reached on the same specimen for a given temperature. The martensite content is evaluated measuring the saturation magnetism on small cuts of tensile sample. The model, well described in [1] can be easily implemented into CAE/CAD software. It was done using ABAQUS (Figure 2b) but also with other codes in the framework of New Generation Vehicle Project [2].

Forming Limit Diagram Prediction

Introductive comments

In a drawing process, the strain state is used to characterize the forming path up to the fracture. Considering conservation of the volume during plastic deformation, the strains in the plane of the sheet, ε_1 and ε_2, are used to characterize this state, and the thinning could be easily deduced. In a diagram (ε_1, ε_2), several deformation modes are encountered. Assuming $\varepsilon_1>0$ for symetry reasons, we have to deal with three locii:

- The drawing area $\varepsilon_2<0$
- Plan strain path $\varepsilon_2 =0$
- The stretching area $\varepsilon_2>0$

The Forming Limit Diagram (FLD) gathers the curves in each domain that separate the safe area during the forming from an area where necking appears and leads to the fracture of sheet. From a practical point of view, the determination of a FLD is very time and cost consuming. Indeed, several deformation tests corresponding to different deformation modes (different ratio $\rho=\varepsilon_1/\varepsilon_2$) have to be performed to determine it (Figure 2). Consequently, many models dedicated to FLD's

prediction have been developed. A Cayssials-type model was developed at ArcelorMittal and adapted to stainless steel [3] and it is summarized in the following paragraph.

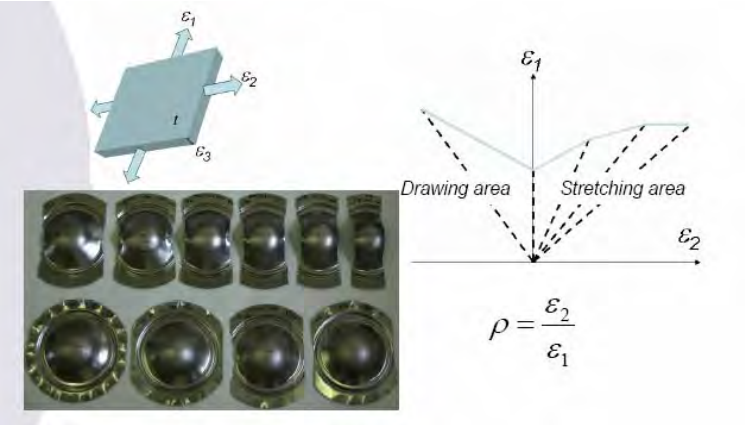

Figure 2. Forming limit diagram principle and Nakazima experimental method for its determination

Proposed FLD model

In the drawing area, the necking boundary is determined by using the instability plastic theory assuming viscoplastic material and necking band occurance (after Hill 1952, Duncombe 1974, Dudzinski & Molinari 1998). For a given path, ε_1 is a function of the hardening coefficient *n* and ε_{10} value at $\varepsilon_2 = 0$ given by the relation $\varepsilon_{10} = a.n+b.m.t$, where *t* and *m* are respectively the thickness and strain rate sensitivity coefficient, *a* and *b* two constants to be indentified. In the stretching area, the mechanism of necking is different and we used the plastic deformation theory, i.e. elastoplasticity with vertex effect and occurance of strain rate gradient jump in the necking band (after Storen & Rice 1975, Hutchinson & Neale 1978). The anisotropy effect in the stretching area was introduced later by Cayssial. Finally the model takes into account four parameters:

- The hardening coefficient (*n*-value): this coefficient is the most important coefficient: an increase of the *n*-value raises the level of the FLD
- The rate sensitivity coefficient (*m*-value): this coefficient has a similar effect as the hardening one, but is less important
- The Lankford parameter (*r*-value): this coefficient has an effect of the second order; when the *r*-value increases, the performances in the stretching area decrease.
- The thickness: an increase of the thickness of the sheet leads to a raise of the FLD's level.

Relation with the measured quantities

Due to different ways of determination of the mechanical properties of ferritic and austenitic stainless steels, the coefficients of the model are different for the two families of grades. In the case of unstable austenitic grades with a strong TRIP-effect, we showed previously that the hardening coefficient cannot be determined easily. On the other hand, it is well known that the necking appears at $\varepsilon = n = ln(1+Ag)$ where *Ag* is the uniform elongation used in the model rather than the *n*-value. Concerning the rate sensitivity coefficient *m*, it can be computed from the Tensile strength *Rm* values by $m = A.Rm^{-B}$. Finally, the constants *a,b,A* and *B* are identified by calibration tests; the model depends on *Rm* strength, *Ag* strain value, *r*-value and the thickness *t*.

Comparison between the model and experiences

We can see in Figure 3 that the Cayssials-type model provides a good prediction of the FLD level. Indeed, for the austenitic grades, 8 cases have been tested (different grades, with different thicknesses). For these 8 cases, we obtained 85% of results with an error lower than 0.03 for the

major strain and 92.5% of results with an error lower than 0.05. Concerning the ferritic grades, 7 cases have been tested. For these 7 cases, we obtained 80% of results with an error lower than 0.03 for the major strain and 100% of results with an error lower than 0.05.

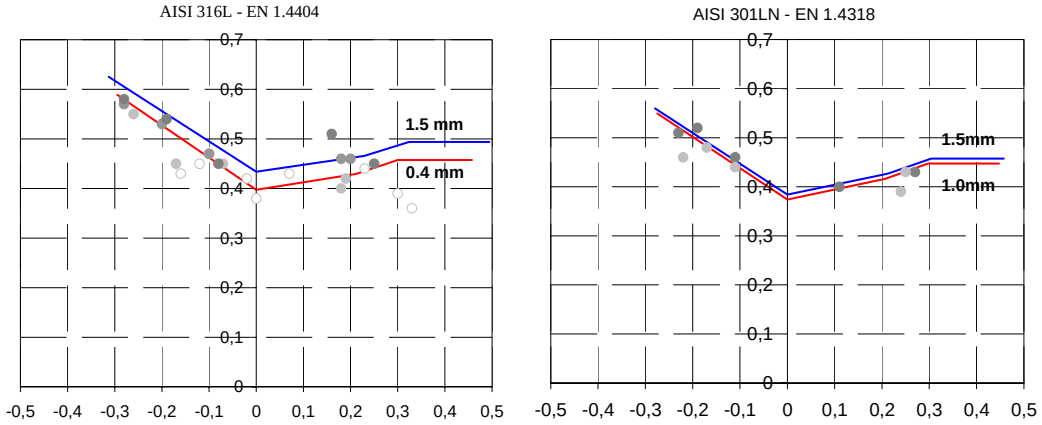

Figure 3. comparison between model and experimental FLD

Conclusion

The proposed model permits to evaluate FLD from tensile test parameters in the 3 directions of the sheet and leads to an accurate prediction. Today we use this predictive model to draw the FLD when it is not available experimentally in our database or when the deadline is too short to performe the characterization. There is still some room for improvement, especially in the case of thin strip (thickness typically less than 0.2mm) because the hypotheses of the model are no longer valid when the thickness becomes of the order of several grain or inclusion sizes, and so the thickness effect is not well described. Moreover, it has been shown in the first part of this paper that unstable austenitic grades are sensitive to the strain rate and even if at this stage we are able to reproduce this behaviour, the sensitivity of the FLD, and more generally of the fracture criterion, is not fitted today with the performed calibration tests.

References

[1] P.O.Santacreu et al. “Behaviour Model of Austenitic Stainless Steels For Automotive Structural Parts” Steel Research Int. 77 (2006) N°9-10, pp. 714-719.

[2] S.Schubert et al. “Next generation vehicle - engineering guidelines for stainless steel in automotive applications” present SS’08 conference G 02-1.

[3] G.Chinouilh et al, “Forming Limit Diagram Prediction of Stainless Steel Sheets”, SAE Technical Paper Serie 2007-01-0338, SAE World Congress, Michigan April 16-19, 2007.

THE α'-MARTENSITE EVOLUTION MATHEMATICAL FORMULATION AND APPLICATION IN THE EARLY DETECTION OF DAMAGE IN SHEET METAL COMPONENTS

B.-A. Behrens, K. Weilandt, M. Kamp, K. Voges-Schwieger

Leibniz Universität Hannover, Germany

Abstract

In this article, a mathematical model for the calculation of martensite evolution in metastable austenitic chrome nickel steels is presented. It considers the transformation-induced martensite evolution depending on temperature, stress, strain and state of stress. The model is based on TSUTA [6] and considers the material's forming history [4]. Deep drawing processes of stainless steels can be precisely simulated by the implementation of this model into the commercial FEA software ABAQUS. This paper deals with the influence of the chemical composition, induced by different batches of material, on the evolution of martensite. Additionally, an application area of martensite evolution is introduced. It is a kind of part-inherent sensor, which allows for timely identification of damage in lightweight constructions. This new non-destructive method for testing, aimed at providing reliability of sheet metal components, is based on the characteristic effects of martensite evolution.

Introduction

Timely identification of damage is of crucial importance for safety components. A new non-destructive method for testing, aimed at providing reliability of sheet metal components in lightweight constructions, is presented. This new method allows for earlier damage identification than conventional visual inspections. It is based on a new concept of part-inherent sensors, which are small areas, plastically deformed by means of metal forming, on a metastable austenitic steel sheet. Due to the plastic deformation, these areas are sensitive to martensite evolution under applied elastic load. This higher sensitivity allows for the correlation between the martensite content in the sensor and the loads it has undergone.

First, the mechanism of martensite evolution and the conducted experimental investigations are described in this paper. Following, a material model considering transformation-induced martensite evolution of metastable austenitic stainless steels is presented. The influence of batches on martensite evolution has been investigated.

Martensite evolution

Because of their high corrosion resistance and deformation characteristics, stainless steels are of high importance for industrial applications. Phase transformation of austenite to martensite occurs during deep-drawing processes; a change in microstructure happens without heat treatment. The martensite evolution causes a rising flow stress and higher strength of the material (Figure 1).

The martensite microstructure can exist in two different lattices. Tetragonally distorted martensite shows a body-centered cubic lattice (bcc), which is called α'-martensite and shows

microstructure characteristics similar to α-ferrite. The ε-martensite is characterized by a hexagonal packing lattice (hcp), but it does not combine the same material properties as α'-martensite, which features high strength and thermo-dynamic stability [3]. Due to these differences in material behavior, the formation of α'-martensite is preferred.
The properties of stainless steels depend on their chemical composition. In this regard, the influence of different batches of the material 1.4301 has to be investigated in particular.

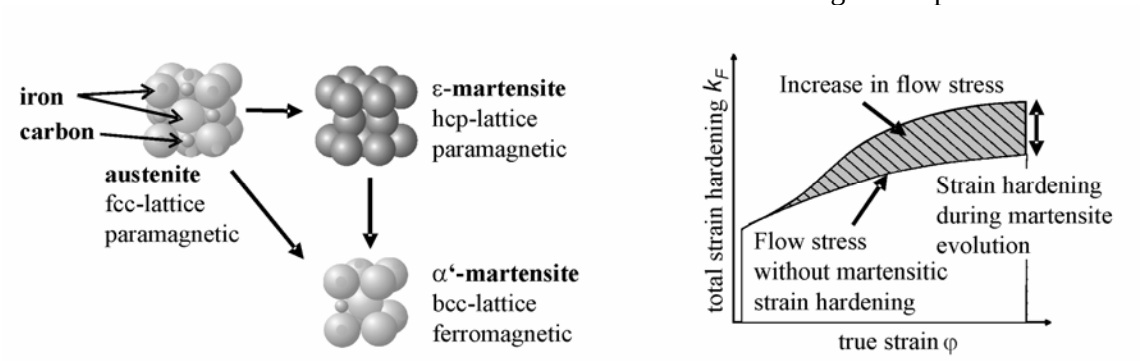

Figure 1. Mechanism of martensite evolution and the caused strain hardening

Experimental investigations and mathematical formulation

Based on numerical and experimental studies involving the metastable austenitic steel X5CrNi18-10, a material model has been developed and qualified at the IFUM [5]. Phase transformation of austenite to martensite occurs during deep-drawing processes, leading to increased strain hardening of the material. The transformation depends on alloying constituents, transformation temperature, stresses, and strains. Consequently, they have to be considered in the design of deep-drawing processes of stainless steels.
Following, a mathematical model for the calculation of the martensite evolution depending on these parameters is presented [SPR05]. This model is based on TSUTA [TSU93] and considers the material's forming history [HAE71]. In detail it includes the formation of α'-martensite depending on the temperature T, the true strain φ, the stress tensor, and the stress condition in terms of the ratio between the principal stresses σ_1/σ_2. The calculation is done incrementally, but mostly independent of certain steps in time. It is based on the following equations (Figure 2), with the material constants A,B,C,D,E,F,G,H. The martensite evolution for the uniaxial stress condition as well as for the biaxial one can be described by this model.

$$\left(\frac{\partial f^{\alpha'}}{\partial \varphi}\left(f^{\alpha'},T,\varphi\right)\right)_{\text{uniaxial}} = \left(1-f^{\alpha'}\right)\cdot\frac{C\cdot\varphi^{-1}}{1-A\cdot e^{D+\frac{B}{T}}\cdot\varphi^{-C}}$$

$$\left(\frac{\partial f^{\alpha'}}{\partial \varphi}\left(f^{\alpha'},T,\varphi,\underline{\underline{\Sigma}}\right)\right)_{\text{biaxial}} = \left(\frac{\partial f^{\alpha'}}{\partial \varphi}\left(f^{\alpha'},T,\varphi\right)\right)_{\text{uniaxial}} + E\cdot\left(1+f^{\alpha' F}\right)\cdot\frac{e^{G-T}}{1+e^{G-T}}\cdot\sqrt{\varphi}\cdot\left(1+H\cdot sigmum\left(\frac{\sigma_2}{\sigma_1}\right)\right)$$

Figure 2. Formulas to describe the martensite evolution for uniaxial and biaxial stresses [SPR05]

The equation for the biaxial stress consists of two summands. The first one is the uniaxial ratio. The second summand is a product of the functions of the relevant influencing factors for the biaxial stress. The considered factors are the microstructure arrangement, the temperature T, the deformation degree φ, and the state of stress σ_1/σ_2.

The microstructure arrangement influences the regeneration mechanism of martensite by using a power function. The temperature is included in the form of a fraction, so that an increasing temperature restrains the martensite evolution. Via square root, a growing deformation degree leads to rising martensite content. The behavior of martensite evolution under tension and pressure is accounted for by means of the last multiplier in the formula Figure 2. Here, tension enhances the α'-martensite formation, while pressure is hindering it.

In the following passage the experimental investigations and the method to gain the material parameters *A, B, C, D, E, F, G, H,* are described. The central aim of this investigation is to quantify the differences of behavior concerning martensite evolution caused by fluctuations between the batches, and thus the transferability for all material batches has to be verified. The flow curve and the martensite fraction of five different batches of the sheet metal material X5CrNi18-10 were derived by uniaxial tensile tests on the testing machine DYNA/Mess S100/ZD available at the IFUM. Two sheet thicknesses (s_0 = 1.0 mm and s_0 = 0.8 mm) were examined. The registration of martensite fraction $f^{\alpha'}$ was based on the magnet inductive measuring method with the aid of the Feritscope® MP3C. The results of the measurements and the approximation are shown in the diagram martensite content versus deformation degree (Figure 3.) The curves for the five batches show differences. Especially batch 1 has a remarkably lower martensite content. Batch 2 and 5 are the samples with the material thickness of s_0 = 0.8 mm.

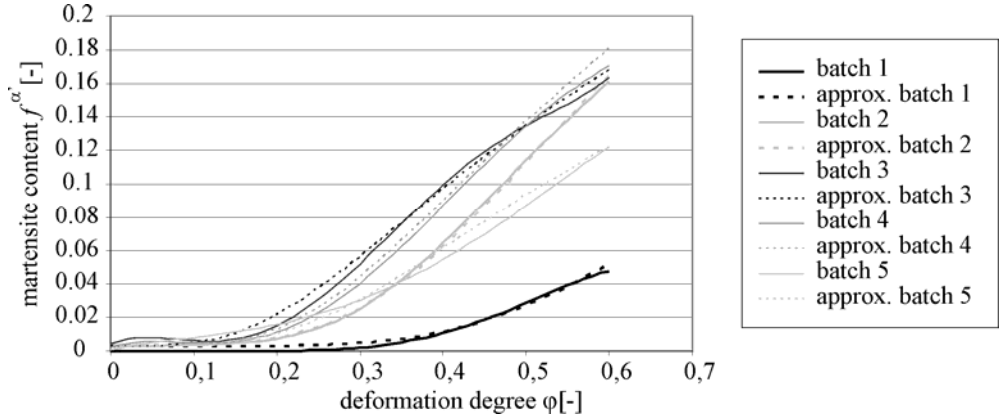

Figure 3. Real and approximated content of martensite for the five batches

The incremental description of the martensite evolution with the constants *A, B, C* , and *D* (Figure 2) was developed in order to be able to describe the martensite evolution in the tensile test. The material parameters of the developed model were determined according to the minimum square deviation method by means of the program Mathematica. A good description of the martensite evolution as a function of the temperature and the plastic strain was obtained using the material parameters in Table 1.

Table 1. Material parameters of the five investigated batches

material	batch	thickness	A	B	C	D	diameter	E	F	G	H
1.4301	1	1 mm	-0.043	-4988	6.24	18.26	200 mm	1.45	0.33	317.15	0.35
1.4301	2	0.8 mm	-6.53E-05	-5000	4.39	24.64	50 mm	1.45	0.33	317.15	0.35
1.4301	3	1 mm	-1.09E-05	-5325	3.63	24.85	50 mm				
1.4301	4	1 mm	-1.09E-05	-5337	4.44	24.18	50 mm				
1.4301	5	0.8 mm	-1.31E-05	-4998	3.89	24.27	50 mm				

In order to quantify the stress-dependence of the martensite evolution, deep-drawn rotationally symmetric cups were analyzed. During the deep drawing process, there are different stress and strain conditions occurring (tensile stresses in radial direction and compression stresses in tangential direction in the flange, plane strain in the wall and tensile stresses in the bottom of the component), whose influence on the martensite evolution has been examined.
The tests using the material of batch 1 with the initial sheet thickness s_0 = 1.0 mm were deep-drawn by a tool with the stamp diameter d_0 = 200 mm. The blank holder force was F_N = 200 kN, and the temperature 20° C. To evaluate the experiments, the deep-drawing force as well as the martensite fraction in the cups were measured. The cups of the material of batch 2 (s_0 = 0.8 mm) were deep-drawn on a rotationally symmetric tool system with the stamp diameter d_0 = 50 mm. The blank holder force was either set to F_N = 50 kN or F_N = 75 kN. The influence of the tensile stresses occurring in the bottom of the cup on the martensite fraction can be examined in these cups. The martensite fraction in the cups was measured magnet-inductively at reference points in the rolling direction. Since the examined stainless steel shows little anisotropy, the martensite fraction is assumed to be similar in the whole cup [1].
The results of the experimental investigations and the curves of the approximation are shown in Figure 4. The investigations show that the martensite content equation for the biaxial stress state (Figure 2) fits with the same material parameters *E, F, G, H* for batches 1 and 2, even though the material behaviour in the uniaxial tensile test shows significant difference.
This leads to the assumption that the influence of the biaxial stress for martensite evolution compensates the differences of the uniaxial one. To verify this statement, the examination of more batches of the material 1.4301 has to be accomplished.

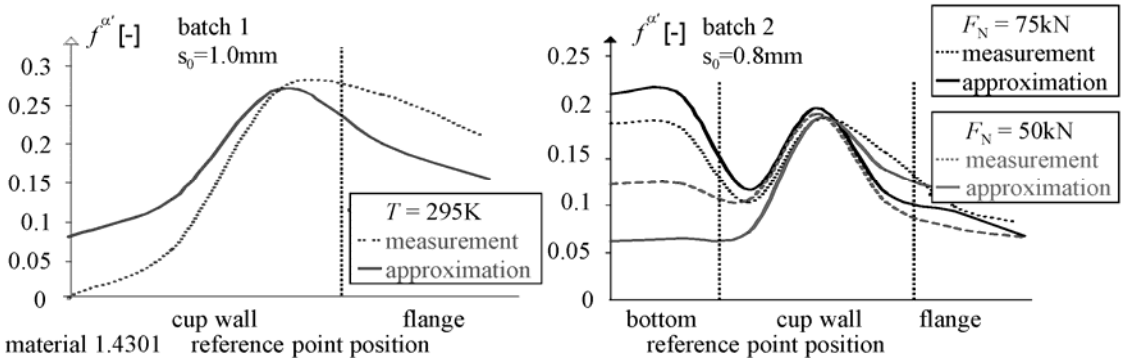

Figure 4. Approximated and measured martensite content over cup contour

Detection of damage in sheet metal components

The mechanism of martensite evolution should be used for a new non-destructive testing method. This new method allows for earlier damage identification than conventional visual inspections, and thus it aims for providing reliability of sheet metal components in lightweight constructions. The idea is to bring small areas of deformation onto a metastable austenitic steel sheet, producing a kind of part-inherent sensor (Figure 5 left.). The plastically deformed areas are implemented by means of metal forming. Due to the plastic deformation, these areas are sensitive to martensite evolution under applied elastic load. This sensitivity allows for the correlation between the martensite content in the sensor and the strains it has undergone (Figure 5 right.).

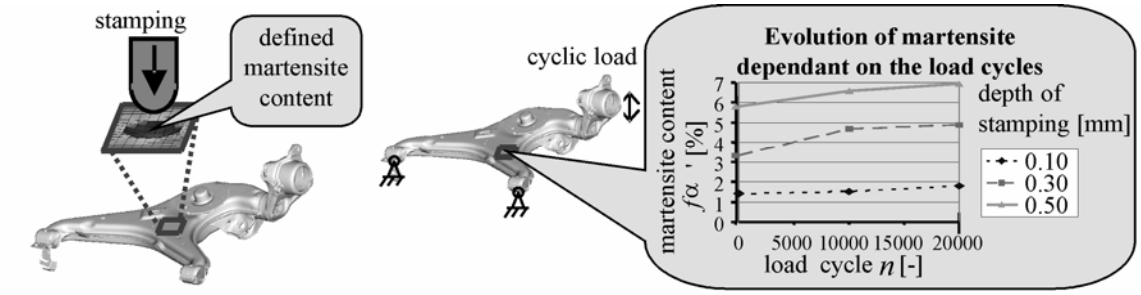

Figure 5 left. Preparation: Induction of locally defined martensite content by stamping
Figure 5 right. Measurement and analysis: Martensite content provides information about loading history

By numerical simulation, various metal forming processes and geometries of the stamp are studied in regard to their ability to influence the desired martensite content. FE models were set up for deep drawing, stretch forming, and stamping, and the results were evaluated (Figure 6.). As a precondition for the adjustment of locally defined initial martensite content, stresses must be applied to the component systematically during the respective forming process.

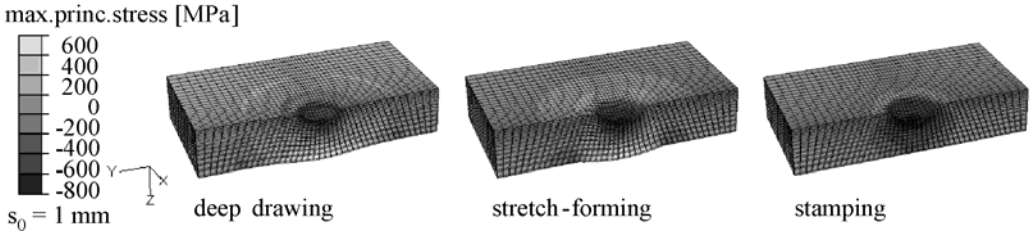

Figure 6. Distribution of the maximal principal stress of the simulated forming processes

The simulations were aimed at localizing the compressive and tensile stresses inside the specimen, so that conclusions about the resulting α'- and ε-martensite areas could be drawn. In order to attain a sensitization of the material, a high evolution of ε- martensite is desirable during the pre-elongation process, since the ε-martensite transforms into α'-martensite by elastic tensile stress. Figure 6 illustrates the favorable stress ratios during the three different forming processes. The intent is to have stable compressive stresses in the stamping area and secondary maximum stresses locally restricted to the stamping position. The results of the simulation clearly indicate that neither the rear side of the stamping position nor the surrounding area is affected by the stamping [2].

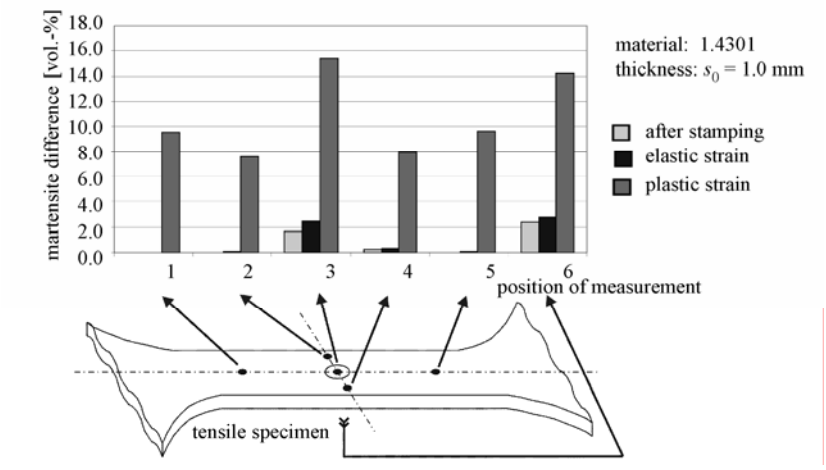

Figure 7. Measured martensite contents on defined positions on the tensile specimen after different loadings

Based on the obtained numerical results, a new stamping tool has been constructed. It allows for the predefinition of specific martensite content in certain areas of the sheets. The martensite content is measured after stamping, elastic and plastic loading on the stamped sheet. As a result, the part-inherent sensors show a higher martensite content than the rest of the sheet (see Figure 7.).
The plan for future works is to develop a model, which allows for a correlation between the local increase of martensite content in the sensors and the load cycles, in order to detect a critical load limit before a failure occurs. Thus, critical components could be exchanged in time.

Conclusions

Martensite evolution is an effect that influences the strain hardening of stainless steel. Especially for the simulation of forming processes, the transformation-induced martensite and the effect of increasing hardening need to be considered, and thus experimental investigations have been evaluated. A mathematical description for the martensite evolution has been analysed, based on the material model of SPRINGUB [SPR05]. This investigation has been performed to clarify the influence of chemical fluctuations caused by different batches on the martensite evolution of the metastabile austenitic steel X5CrNi18-10 (EN 1.4301). The results show that the martensite content equation for the biaxial stress state (Figure 2) fits with the same material parameters *E, F, G, H* for the batches 1 and 2, even though the material behaviour in the uniaxial tensile test shows significant difference. The research concerning the application of martensite evolution in the detection of damage has just begun, but so far promising results have been gained. The effect of martensite evolution by elastic strain in pre-deformed areas is certified, and thus a basis for further investigations is provided.

References

[1] Behrens, B.-A.; Doege, E. ; Springub, B. “Transformation induced martensite evolution in metal forming processes of stainless steels”; steel research int. 75, 7/2004

[2] B.-A. Behrens, M. Kamp, K. Weilandt: “Umformtechnisches Verfahren zur Sensibilisierung der Martensitbildung unter elastischer Belastung”, Metall, Heft 3, Giesel Verlag, 2007

[3] D. Goodschild, W. T. Roberts and D. V. Wilson: “Mechanical behaviour of textured austenitic stainless steel”, Journal of the Iron and Steel Institute, 1971, pp. 283-290

[4] Hänsel, A.H.C.; Hora, P.; Reissner, J.: “Model for the kinetics of strain-induced martensitic phase transformation at non isothermal conditions for the simulation of sheet metal forming processes with metastable austenitic steels, Simulation of Materials Processing”: Theory, Methods and Applications, Rotterdam, 1998.

[5] Springub, B.: „Semi-analytische Betrachtung des Tiefziehens rotationssymmetrischer Bauteile unter Berücksichtigung der Martensitevolution“, Ph.D. dissertation, Universität Hannover, 2005.

[6] Tsuta, T.; Cortes R., J.A.: “Flow Stress and Phase Transformation Analyses in Austenitic Stainless Steel Under Cold Working”, Part 2, JSME International Journal, Serie A, 36. Band, 1993, Vol 1, S. 63-72.

GRAIN REFINED STRUCTURE OF 304 STAINLESS STEEL BY SHORT ANNEALING AFTER SEVERE DEFORMATION

A. Lis, J. Lis, P. Wieczorek, K. Kiera-Beleć

Częstochowa University of Technology, Poland

Abstract

Stainless steel Type 304 was deformed 65.9% by wire drawing to 3,3 mm diameter and then annealed in a dilatometer furnace at 973 K for 100 s. Reversion from deformation induced martensite to austenite via the shear mechanism combined with recocery and recrystallization process was confirmed by transmission electron microscopy investigations. Tensile tests were done at temperature 293 down to 77 K. Transformation induced plasticity effect of austenite to martensite was observed in tensile tests at low temperatures. TEM observations revealed microstructural changes caused by deformation. Formation of martensite on shear band and twin intersections was noticed. The recovered strucures of martensitic ferrite and new small austenite grains with the diameter less than 2.2 μm were observed in annealed specimens. The thermomechanical procedure for production of high strength and ductile 304 stainless steel wires was proposed.

Introduction

Grain refining processes are greatly varying depending on the reversion mechanism. Martensitically reversed austenite has a high density of dislocations imediately after the reversion and the austenite grains are refined through recovery and recrystallization processes just like that taking place in deformed austenite. On the other hand, diffusionally reversed austenite is characterised by the nucleation of equiaxed austenite grains within the α' matrix and then the austenite grains gradually grow during annealing [1]. Processing of submicron grained microstructures and enhanced mechanical properties by cold-rolling and reversion annealing of metastable austenitic stainless steels was presented in paper [2].

In the present work, microstructural features of reversed austenite were investigated after cold drawing with 65.9% reduction from 5.65 mm to 3.3 mm. As will be shown α' reverts to austenite on annealing at 973 K for 100s via both reversion mechanisms. Tensile tests up to fracture at room temperature 293 K and after subzero treatment were done.Also TRIP effect was studied during tensile deformation at liquid nitrogen temperature 77 K at which austenite almost completely transforms to α' martensite.

Experimental

The commercial austenitic stainless steel Type 304 was chosen for this study. Its composition is listed in Table 1. The austenite stability index, M_{d30} temperature, as proposed by Nohara et al. [3] was calculated, and it equals to 34.3 ^{0}C (307.3 K).

Table 1. Chemical composition of the tested steel Type 304 (in mass %)

C [%]	N [%]	Cr [%]	Ni [%]	Mn [%]	Si [%]	Cu [%]	Mo [%]
0,05	0,01	18,04	8.17	1,84	0,43	0,32	0,30

Cylindrical tensile specimens 8 x 78 mm were machined from cold drawn bar Φ 16 mm. The mechanical properties were established using tensile test machine MTS which had the attachment for low temperature testing at temperatures: 293, 273, 253, 233, 213, 193, 173 and 77 K. The test results are given in Table 2.

Table 2. Static tensile tests results

Temp (K)	EL (%)	RA (%)	YS (MPa)	TRIP (MPa)	TS (MPa)
293	50.0	76.7	476	-	760
273	56.0	74.6	508	-	867
253	52.2	74.7	528	-	953
233	46.6	72.4	515	659	1020
213	41.9	71.2	506	650	1048
193	43.0	71.1	530	634	1132
173	41.1	67.8	515	641	1241
77	29.3	60.0	562	703	1671

At temperatures 233 K, down to 77 K, a horizontal plateau of stress was observed on stress – strain curves (Figure 1). This is assumed to be due to the occurrence of TRansformation Induced Plasticity effect of the austenite to martensite transformation. Thus stress TRIP has also been given (Table 2). With decreasing testing temperature, the stronger TRIP effect was observed, with considerable plastic strain at constant stress level. In Figure 2, stress – strain curve obtained at room temperature is compared to the one recorded at 77 K. In the latter case strain hardening is extremely strong reflecting a high instablity of the austenite and formation of the strain induced martensite. Thus the maximum value of the tensile strength 1671 MPa was obtained at this temperature. This phenomenon was not observed at room temperature. Moderate strain hardening was from increased dilocation density, shear bands and twinning effects observed in the austenite microstructure in thin foils with transmission electron microscope Philips 301G – Figure 3. Microstructure of the deformed martensite in the sample tensile tested at 77 K is presented in Figure 4. Due to low temperature straining strain induced martensite is present in the structure. Lath martensite and dislocations cell regions were observed.

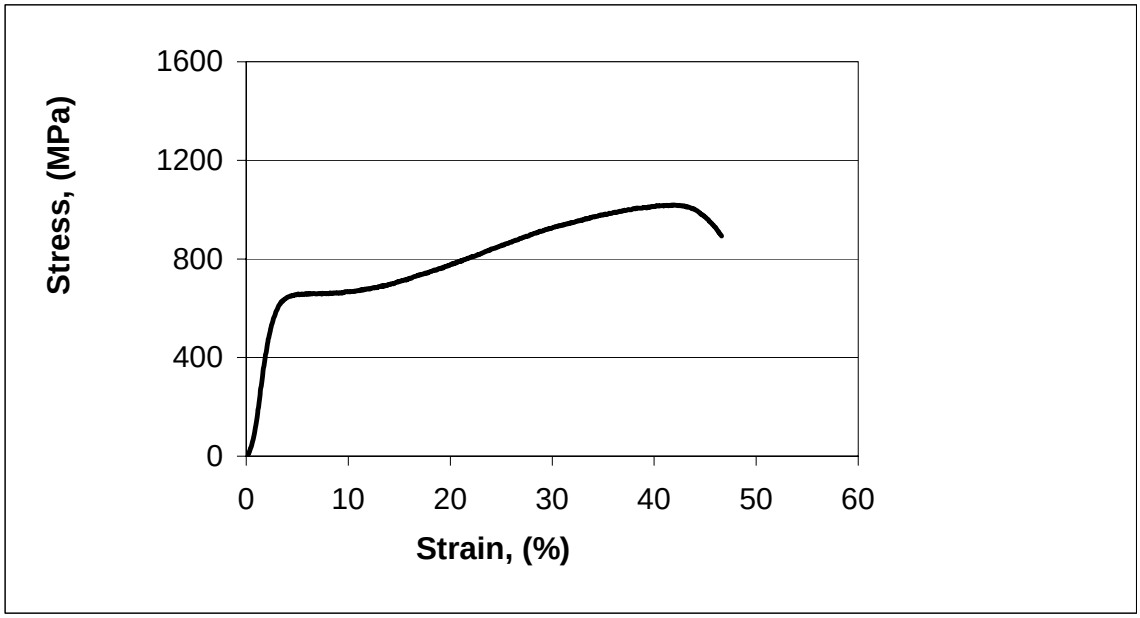

Figure 1. Stress-strain curve of Type 304 steel at 233 K

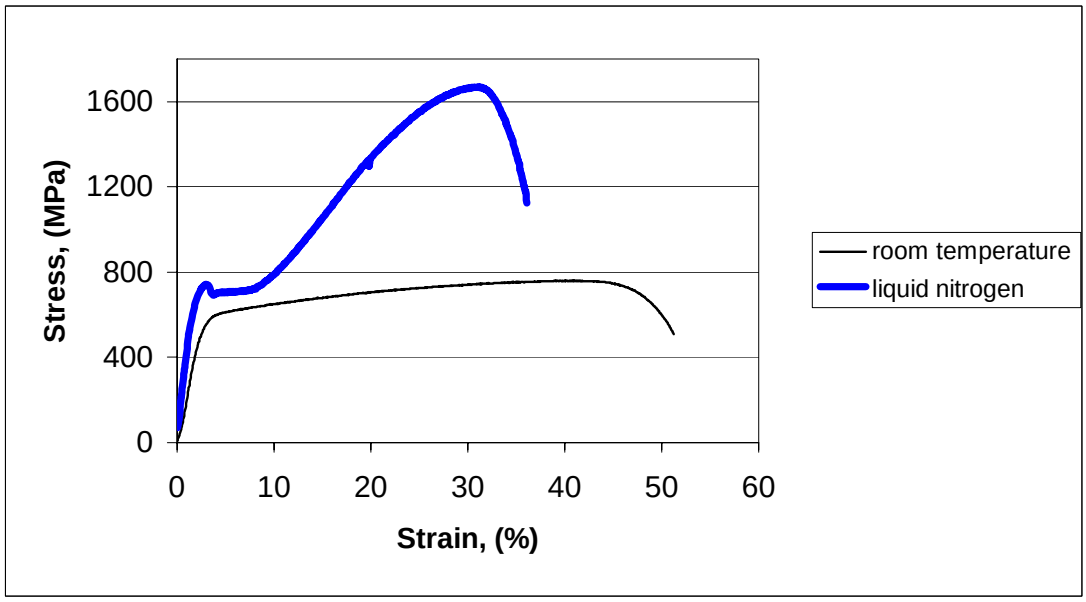

Figure 2. Stress-strain curves of Type 304 steel at 293 K and 77 K

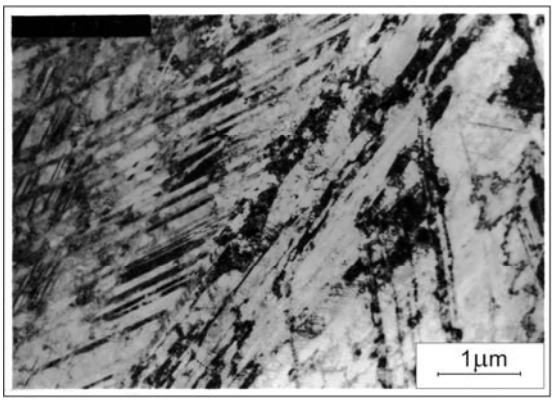

Figure 3. Microstructure after static tensile test at the temperature 293 K, TEM

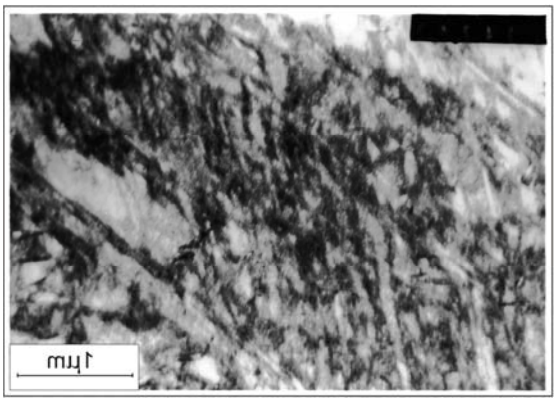

Figure 4. Microstructure after static tensile test at the temperature 77 K, TEM

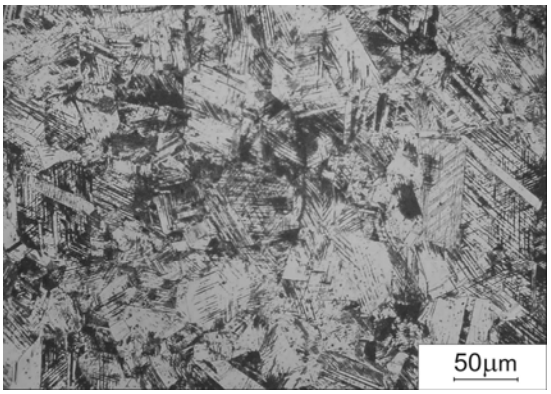

Figure 5. Austenitic structure of the sample in the initial state, temperature 293 K, OM

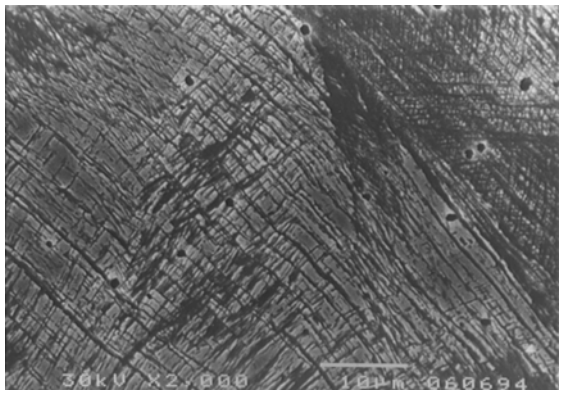

Figure 6. Microstructure after drawing to 3,3 mm, deformation 65.9%, SEM

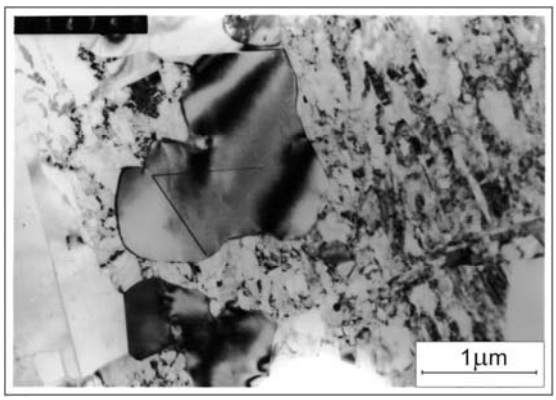

Figure 7. Microstructure after annealing at the temperature 973 K/100s, TEM

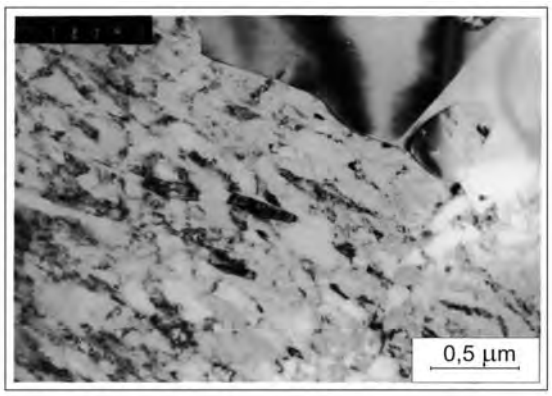

Figure 8. Microstructure after annealing at the temperature 973 K/100s, TEM

The initial microstructure of 304 steel after cold drawing as observed in optical microscope is shown in Figure 5. Dense mechanical twinning is observed within austenite grains. The maximum twin length was about 25-86 µm. The intersections of twins and shear bands where α' martensite nucleates are clearly visible at 2000 x magnification in scanning electron microscope in Figure 6. Such microstructure was obtained after cold drawing in five passes the bar from Φ 5.65 mm to the wire Φ 3.3 mm i.e. reduction 65.9%. After cold drawing, the wire was annealed at 973 K for 100 s in a dilatometer furnace. Heating and cooling rate was 20°C/s.

At relatively high temperatures of 973 – 1173 K, after the α'→γ transformation, conventional static recrystallization occurs which involves the nucleation and growth of dislocation free grains. These grains have dislocation densities several orders of magnitude lower than in the deformed matrix of recovered α'martensite. Non-uniform sized microstructure existing after 973 K/100 s annealing is presented in Figures 7 and 8. There are few austenite grains of the order 2 μm with a small number of recrystallization twins but also very fine austenite grains at recovered regions in the form of lathes which width is in the range of 50- 150 nm. Volume fraction of the very fine grains is about 60%. This type of microstructure has presumably high strength and good ductility.

Conclusions

- In tensile testing of Type 304 stainless steel TRIP effect was observed at low temperatures below 233 K down to 77 K.
- The shape of the stress- strain tensile curve at 77 K indicates intensive martensite formation, while at room temperature moderate hardening is rather due to increase of dislocations and twinning effect in austenite.
- Strain induced martensite is formed during cold drawing at reduction 65.9% which increases the strength, but the elongation is significantly reduced. Further drawing is impossible.
- After annealing at 973 K for 100 s the microstructure is composed of fine austenite grains which are diffusionally nucleated and grown to the size of about 2 μm and also ultra fine high – dislocated shear reverted austenite which has laths of 0.15 μm in width.

References

[1] K. Tomimura, S. Takaki, Y. Tokunaga, " Reversion Mechanism from Deformation Induced Martensite to Austenite in Metastable Austenitic Stainless Steels", ISIJ International, 31, 12, 1991, pp. 1431- 1437.

[2] M.C. Somani, L. P. Karjalainen, A. Kyröläinen and T. Taulavuori, "Processing of submicron grained microstructures and enhanced mechanical properties by cold rolling and reversion annealing of metastable austenitic stainless steels, Materials Science Forum Vols. 539-543, 2007, pp.4875-4880.

[3] Nohara, Y. Ono, N.J. Ohashi, Strain – Induced Martensitic Transformation in Metastable Austenitic Stainless Steels in Multi-Stage Tensile Deformation at various Temperatures, Proceedings of the First JIM International Symposium on New Aspects of Martensitic Transformation, Kobe, May 1976, The Japan Institute of Metals, pp. 315-320.

THRESHOLD BEHAVIOR OF FeCr ALLOYS SURFACE

M. Ropo[1,2], K. Kokko[1], M.P.J. Punkkinen[1], S. Hogmark[3], J. Kollár[4], B. Johansson[2,3,5], L. Vitos[2,3,4]

[1]University of Turku, Finland, [2]Royal Institute of Technology, Sweden, [3]Uppsala University, Sweden, [4]Research Institute for Solid State Physics and Optics, Hungary, [5]School of Physics and Optoelectronic Technology & College of Advanced Science and Technology Dalian University of Technology, China

Abstract

The surface concentration profile for iron rich Fe-Cr alloys in vacuum was determined using atomistic modelling based on first principles quantum theory. The surface Cr concentration show peculiar threshold behaviour, in dilute alloys the surfaces are covered exclusively by Fe, whereas for bulk Cr concentrations above ~10% the Cr-containing surface becomes favourable. The two dissimilar regimes appear as a consequence of competing magnetic effects: the magnetically induced immiscibility in bulk Fe-Cr alloys and the stability of magnetic surfaces.

Introduction

In the Fe-Cr alloys, the transition from the iron-type to noncorrosive behaviour with increasing chromium content occurs in the narrow concentration interval of 9-13% Cr [1]. Despite its fundamental role in stainless steels, the origin of this threshold behaviour is not well understood. Numerous experimental studies have been focused on the chemistry of the Fe-Cr surfaces at ultrahigh vacuum conditions as well as on the formation of the protecting Cr-rich oxide layers [2,3,5]. However, these experiments were performed on commercially important alloys (i.e. bulk Cr content above 12%), and therefore were unable to reveal the concentration profile as a function of bulk composition. On the theoretical side, all investigations considered dilute alloys and predicted the stability of Cr-free surfaces [4,6,7]. Therefore, the knowledge about how the chemical composition changes in $Fe_{1-c}Cr_c$ alloys when going from the low-Cr regime (c<0.1) to the high-Cr regime (c>0.1) has been very scarce.

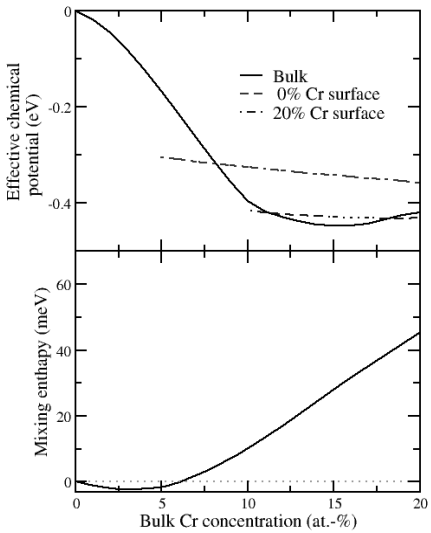

Figure 1. Upper panel, the effective chemical potentials for bulk and two surfaces with different chemical composition. Lower panel, the mixing enthalpy of disordered Fe-Cr alloy. All graphs are presented as a function of bulk Cr concentration.

Method

Our ability to address the above problem at a first-principle quantum mechanical level has become possible through the exact muffin-tin orbital (EMTO) [8] method based on density functional theory [9] in combination with the generalised gradient approximation [10]. This approach has proved to be an accurate tool to describe the Fe-based random alloys [11,12].

The surface concentrations were obtained by minimising the grand canonical potential of the surface. This leads to condition that the difference between effective chemical potentials (ECPs) for the surface alloy ($\Delta\mu_S$) and bulk alloy ($\Delta\mu_B$) should be equal, $\Delta\mu_S = \Delta\mu_B$. The ECPs were derived from the free energy calculated separately for the bulk and surface systems. The entropy part of the free energy was approximated by the configurational entropy. For Fe-rich alloys and for temperatures well below the magnetic transition temperature (~950 K for iron rich Fe-Cr alloys), the magnetic and vibrational entropy terms are estimated to have negligible effect on the equilibrium concentration profile [13]. More details about the calculations can be found in our previous publications [14,15].

Results

Upper panel of Figure 1 shows the bulk and surface effective chemical potentials at 0 K as a function of bulk composition. The chromium containing surface becomes stable in the alloy when $\Delta\mu_S > \Delta\mu_B$, i.e., where it is energetically more favourable to place Cr atom to the surface than in the bulk. The corresponding chemical profile is shown in Figure 2. From this figure a clear transition from pure Fe surface to Cr containing surface can be seen, which occurs around 8 at.-% Cr in the alloy. At lower Cr concentrations there is practically no Cr present at the surface. It is interesting that the transition is due to the drastic decrease of the effective chemical potential in the bulk rather than to any marked surface effect.

The predicted stability of Cr enriched surfaces in the stainless region is fully supported by experiments[3,5]. A quantitative comparison shows that the present theoretical surface Cr content is below the observed values of 45% and 69% for 13% and 25% Cr in the bulk alloy. However it is important to note that these experiments were performed on samples heated to

973 K under ultrahigh vacuum. At this temperature, the Fe-Cr alloys are close to their magnetic transition, which has a substantial effect on the thermodynamics of bulk and surface alloys [16]. This will become clear if we understand the mechanism responsible for the stability of Cr-containing surfaces in ferromagnetic alloys.

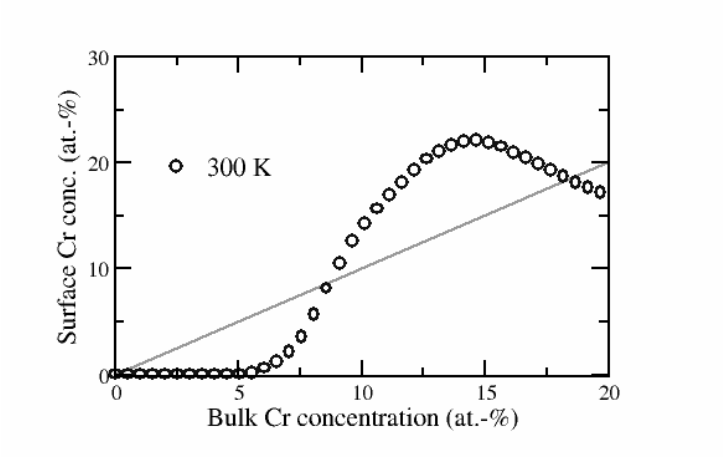

Figure 2. The surface concentration of Cr as function of bulk Cr concentration. Solid grey line shows a linear trend (a homogenous alloy).

The drastic changes in the effective chemical potential for bulk is due to the broad and skewed miscibility gap, allowing solubility of the small amount Cr in Fe but not vice versa (Lower panel, Figure 1). The limited solubility of chromium in iron is due to the complex magnetic interactions between ferromagnetic Fe and antiferromagnetic Cr in Fe-Cr alloys [4,16,17,18]. These interactions originate from magnetic frustration due to the strong anti-parallel coupling between Cr and the Fe matrix and also between different Cr atoms.[4] The energetically unfavourable magnetic interactions between parallel Cr atoms can be avoided or minimised by forming Cr rich clusters and moving some Cr atoms to the surface.
Based on the above mechanism, we can easily give a qualitative explanation for the deviation between the present theoretical (Figure 2) and former experimental results [3,5]. Assuming that the magnetic transition temperature near the surface is below the bulk transition temperature, at elevated temperatures we face the situation when Cr should segregate from ferromagnetic bulk to paramagnetic surface. In paramagnetic alloys, the mixing enthalpy has a markedly different shape than in ferromagnetic case [19]. Because of that and because of the increased effective chemical potential for paramagnetic surface compared to that obtained for ferromagnetic surface [20], our mechanism would predict a significantly stronger Cr segregation to the surface above the surface magnetic transition temperature.

We conclude that the magnetic driven solubility of Cr in Fe is in fact the main factor responsible for the stability of Cr containing surfaces in iron rich Fe-Cr alloys. The magnetic interactions in the bulk has been proposed to have decisive role in properties of the Fe-Cr alloys in several theoretical investigations [4,16,17,18,21], but the impact on the surface chemical composition has not been revealed before our investigations on the matter [15]. We have disclosed an atomistic scenario based exclusively on thermodynamics, which might be a key driving force behind the experimentally observed threshold behaviour in Fe-Cr system [1]. The presence of Cr at the surface enables the formation of protective surface layer in oxidising environment. However, below the compositional threshold, Fe terminated surfaces are favourable and therefore the formation of protective Cr oxide layer is hindered. Obviously, the presence of oxygen will alter the above scenario based only on bulk reservoir. However, even in these more realistic situations, where the kinetic effects become crucial, the proposed thermodynamic mechanism will play a fundamental role in the surface chemistry of Fe-Cr system.

References

[1] G. Wranglén: An introduction to Corrosion and Protection of Metals, New York, 1985.
[2] E. Park, B. Hüning and M. Spiegel, Appl. Surf. Sci., 249, 2005, p. 127
[3] J. R. Lince, S. V. Didziulis, D. K. Shuh, T. D. Durbin and J. A. yarmoff, Surf. Sci. 277, 1992, p. 43
[4] B. Nonas, K. Wildberger, R. Zeller and P. H. Dederichs, Phys. Rev. Lett., 80, 1998, p. 4574
[5] S. Suzuki, T. Kosaka, H. Inoue, M. Isshiki and Y. Waseda, Appl. Surf. Sci., 103, 1996, p. 495
[6] A. V. Ruban, H. L. Skriver and J. K. Norskov, Phys. Rev. B, 59, 1999, p. 15990
[7] A. V. Ponomarave, E. I. Isaev, N. V. Skorodumova, Yu. Kh. Vekilov and I. A. Abrikosov, Phys. Rev. B, 75, 2007, p. 245406
[8] L. Vitos, I. A. Abrikosov and B. Johansson, Phys. Rev. Lett., 87, 2001, p. 156401
[9] P. Hohenberg and W. Kohn, Phys. Rev., 136, 1964, p. B864
[10] J. P. Perdew, K. Burke and M. Ernzerhof, Phys. Rev. Lett., 77, 1996, p. 3865
[11] L. Vitos, P. A. Korzhavyi and B. Johansson, Nat. Mater., 2, 2003, p. 25
[12] L. Dubrovinsky *et al.*, Nature, 422, 2003, p. 58
[13] B. Fultz, L. Anthony, J. L. Robertson, R. M. Nicklow, S. Spooner and M. Mostoller, Phys. Rev. B, 52, 1995, p. 3280
[14] M.Ropo, K. Kokko, L. Vitos and J. Kollár, Syrf. Sci., 600, 2006, p. 904
[15] M. Ropo, K. Kokko, M. P. J. Punkkinen, S. Hogmark, J. Kollár, B. Johansson and L. Vitos, Phys. Rev. B, 76, 2007, p. 220410(R)
[16] P. Olsson, I. A. Abrikosov and J. Wallenius, Phys. rev. B, 73, 2006, p. 104416
[17] G. J. Ackland, Phys. Rev. Lett., 97, 2006, p. 015502
[18] P. Olsson, C. Domain and J. Wallenius, Phys. Rev. B, 75, 2007, p. 014110
[19] A. E. Kissavos, S. I. Simak, P. Olsson, L. Vitos, and I. A. Abrikosov, Comp. Mat. Sci. **35**, 2006, 1
[20] M. Ropo, K. Kokko, L. Vitos, unpublished
[21] T. P. C. Klaver, R. Drautz and M. W. Finni, Phys. Rev. B, 74, 2006, p. 094435

STACKING FAULT ENERGIES OF AUSTENITIC STAINLESS STEELS FROM FIRST-PRINCIPLES THEORY

L. Vitos[1,2], P. A. Korzhavyi[2], J.-O. Nilsson[3,4], B. Johansson[1,2,5]

[1]Royal Institute, Sweden, [2]Uppsala University,Sweden, [3]University of Technology and Göteborg University,Sweden, [4]AB Sandvik Materials Technology, Sweden, [5]School of Physics and Optoelectronic Technology & College of Advanced Science and Technology Dalian University of Technology, China

Stainless steels are among the most important engineering materials, finding their principal scope in industry, specifically in cutlery, food production, storage, architecture, medical equipment, etc. Austenitic stainless steels form the largest sub-category of stainless steels. Fully austenitic grades are composed mainly of Fe, Cr, and Ni, and have the face centered cubic structure of γ-Fe. At low temperatures, these alloys exhibit a rich variety of magnetic structures as a function of chemical composition, ranging from ferromagnetic phase to spin-glass and antiferromagnetic alignments. At ambient conditions, the austenitic steels have very low magnetic permeability and are generally regarded as non-magnetic. Because of this, they represent the primary choice for non-magnetic engineering materials.

The presence of the chemical and magnetic disorder hindered any previous attempt to calculate the fundamental electronic, structural and mechanical properties of austenitic stainless steels from first-principles theories. Our ability to reach an *ab initio* atomistic level in this exiting field has become possible by the recently developed Exact Muffin-Tin Orbitals (EMTO) method [1-3]. This method, in combination with the coherent potential approximation [4], has proved an accurate tool in the ab initio description of the concentrated random alloys [1,5-9]. During the last few years, using the EMTO method, we presented an insight to the electronic and magnetic structure, and micromechanical properties of austenitic stainless steels [7-10]. In the present contribution, using the EMTO method, we will reveal the role of (para-) magnetism on the stacking fault energy of austenitic steels.

References

[1] L. Vitos, Computational Quantum Mechanics for Materials Engineers: The EMTO Methodand Applications. Springer-Verlag London, Series: Engineering Materials and Processes (2007).
[2] O. K. Andersen, O. Jepsen, and G. Krier, in Lectures on Methods of Electronic Structure Calculations, edited by V. Kumar, O. K. Andersen, and A. Mookerjee,World Scientific Publishing Co., Singapore, pp. 63-124 (1994).
[3] L. Vitos, Phys. Rev. B 64 (2001) 014107.
[4] L. Vitos, I. A. Abrikosov, B. Johansson, Phys. Rev. Lett. 87 (2001) 156401.
[5] L. Dubrovinsky, L., et al. Nature 422 (2003) 58.

[6] L. Dubrovinsky, L., et al. Science 316 (2007) 1880.
[7] L. Vitos, P. A. Korzhavyi, B. Johansson, Nature Materials 2 (2003) 25.
[8] L. Vitos, P. A. Korzhavyi, B. Johansson, Phys. Rev. Lett. 88 (2002) 155501.
[9] L. Vitos, P. A. Korzhavyi, B. Johansson, Phys. Rev. Lett. 96 (2006) 117210.
[10] L. Vitos, J.-O. Nilsson, B. Johansson, Acta Materialia 54 (2006) 3821.